

Measurement of the acceptance by means of transverse beam excitation with noise

S. Sorge,* G. Franchetti, and A. Parfenova

GSI Darmstadt, Planckstraße 1, 64291 Darmstadt, Germany

(Received 16 September 2009; published 31 May 2011)

In this work, we present a technique to measure the acceptance of a circular accelerator extending a previous method by the measurement of particle loss. Here, we apply an rf voltage to transversely excite a coasting heavy ion beam in the SIS-18 synchrotron at GSI. The resulting growth of the transverse beam width causes particle loss when the beam width exceeds the limiting aperture. The acceptance is determined from the measured time evolution of the beam current after particles start to hit the aperture. In doing so, the result will not depend on the initial width of the ion beam.

DOI: 10.1103/PhysRevSTAB.14.052802

PACS numbers: 02.70.Ns, 29.20.dk, 29.27.-a

I. INTRODUCTION

The heavy ion synchrotron SIS-18 at GSI [1,2] is used for providing a large variety of heavy ions. Beam energies up to about 1 GeV/u for U^{73+} ions and 4.5 GeV for protons are achievable. The variety of requirements concerning the operation, in particular, the usage of SIS-18 as a booster within the FAIR project [2,3] underway at GSI, also includes regular operation in a high-current regime. In this regime, uncontrolled beam loss in the pipe can lead to irradiation of the machine and vacuum degradation with a sensible reduction of the beam lifetime [4,5]. A precise knowledge of the SIS-18 acceptance will help to optimize the linear optics, which is the first step towards an improved beam loss control.

Limitations of the acceptance are caused by the accelerator optics of the injection scheme [6]. The integrated sum of all errors from the linear optics causes a reduction of the acceptance. Although the acceptance can theoretically be computed via particle tracking simulations, the lack of knowledge of an accelerator under real working conditions makes it desirable to develop a method for measuring the acceptance with beam.

Several experiments, which used the diffusion process, had been performed at different accelerators to measure the acceptance or the dynamic aperture. The particle diffusion was obtained by either using noise applied transversely to the beam [7] or using the ripple in the field of the magnets [8]. The latter method led to a stochastic detuning of the particles which generates transverse diffusion. The acceptance was determined from the measured time required for the beam edge to reach the aperture. Unfortunately, the estimation of this time had a large uncertainty because a detailed knowledge of the initial beam size was necessary

which translated into a large uncertainty in the derived acceptance.

In order to avoid this uncertainty we study how the loss of particles evolves after they reach the limiting aperture of the accelerator. This means that the beam loss evolution is determined by stochastic dynamics rather than by the initial particle distribution. It can be shown that the integrated effect of the stochastic or pseudostochastic transverse rf voltage transforms any arbitrary initial particle distribution into the same asymptotic distribution allowing the determination of the accelerator acceptance.

This paper is organized into the following: Sec. II contains the derivation of an analytical model describing the growth of the beam size as a diffusion process driven by white noise. In Sec. III, the emittance growth and particle loss generated by a realistic rf field are discussed. In Sec. IV, a tracking model is introduced and compared to the diffusion model. In Sec. V the experimental data are presented and compared with results from simulations. Finally, the SIS-18 acceptance is determined from the data. The paper is concluded with a summary in Sec. VI and with Appendix A on the beam emittance growth due to white noise and Appendix B on the analysis and estimation of the acceptance error due to uncertainties in the lattice and beam parameters.

II. DIFFUSION MODEL

A. Particle loss

The method to measure the acceptance is based on the measurement of the time evolution of the beam current which is affected by noise driven beam loss. The noise propagates particles from regions of high density to weakly populated regions as shown by the equation

$$\vec{j} = -C\nabla f, \quad (1)$$

where only the motion in vertical phase space is considered. In Eq. (1), f is the particle distribution function in the vertical phase space plane and ∇ is the vector differential operator acting on the vertical normalized phase space

*S.Sorge@gsi.de

Published by the American Physical Society under the terms of the Creative Commons Attribution 3.0 License. Further distribution of this work must maintain attribution to the author(s) and the published article's title, journal citation, and DOI.

coordinates $(y, p_y) = (y, \beta_y y' + \alpha_y y)$, where α_y, β_y are the Twiss parameters. C is the diffusion constant. Inserting Eq. (1) into the continuity equation

$$\frac{\partial f}{\partial t} = -\nabla \cdot \vec{j} \quad (2)$$

yields the diffusion equation

$$\frac{\partial f}{\partial t} = C \nabla^2 f. \quad (3)$$

Equation (3) can be used to calculate the beam growth and the resulting particle loss. To show that, we follow chapter 7.2 in Ref. [9] and restrict the discussion to an initial particle distribution function dependent only on the Courant-Snyder invariant $\epsilon = (y^2 + p_y^2)/\beta_y$. This invariant is equal to the emittance of a particle. Furthermore, it is shown in Ref. [9] that C can be replaced with $\beta_y(d\epsilon_{av}/dt)/4$ to include processes which occur at several locations in the ring, where ϵ_{av} is the emittance averaged over all particles in the beam. The diffusion equation in terms of emittances becomes

$$\frac{\partial f}{\partial t} = \left(\frac{d\epsilon_{av}}{dt}\right) \frac{\partial}{\partial \epsilon} \left(\epsilon \frac{\partial f}{\partial \epsilon}\right). \quad (4)$$

This equation has to be solved for the boundary conditions

$$f(\epsilon = \epsilon_{lim}, t) = 0 \quad \text{and} \quad f(\epsilon, t = 0) = f_0(\epsilon), \quad (5)$$

where the first constraint means that a particle becomes lost when its emittance ϵ reaches the acceptance ϵ_{lim} . The general solution to Eq. (4) is

$$f(\epsilon, t) = \sum_{n=1}^{\infty} c_n J_0 \left(\lambda_n \sqrt{\frac{\epsilon}{\epsilon_{lim}}} \right) \exp \left[-\frac{\lambda_n^2}{4} \left(\frac{d\epsilon_{av}}{dt} \right) \frac{t}{\epsilon_{lim}} \right] \quad (6)$$

with $0 \leq \epsilon \leq \epsilon_{lim}$. Here, c_n are constant coefficients determined by $f_0(\epsilon)$, J_0 is a Bessel function, and λ_n are the zeros of J_0 . Note that $f(\epsilon, t)$ is a solution to Eq. (4) only if the condition

$$\frac{d\epsilon_{av}}{dt} = \text{const} \quad (7)$$

is fulfilled. This can be proven by inserting the right-hand side of Eq. (6) into Eq. (4) and requiring that J_0 be a solution to Bessel's equation, $x^2 J_0'' + x J_0' + x^2 J_0 = 0$. It will be shown in the following section that $d\epsilon_{av}/dt$ is a constant which is independent of the initial particle distribution.

The summands on the right-hand side of Eq. (6) decrease exponentially in time with the characteristic time for the decrease determined by the λ_n . λ_1 is the smallest zero of J_0 . Therefore, the first summand decreases much slower than all other terms. When t becomes sufficiently large so that the condition $(d\epsilon_{av}/dt)(t/\epsilon_{lim}) \sim 1 + \ln|c_{n,max}/c_1|$ is approximately fulfilled, $f(\epsilon, t)$ will essentially be given by its first summand. Here, $c_{n,max}$ denotes the coefficient with the largest modulus. In this case the distribution function approximately reads

$$f(\epsilon, t) \propto J_0 \left(\lambda_1 \sqrt{\frac{\epsilon}{\epsilon_{lim}}} \right) \exp \left[-\frac{\lambda_1^2}{4} \left(\frac{d\epsilon_{av}}{dt} \right) \frac{t}{\epsilon_{lim}} \right]. \quad (8)$$

The exponential function causes only an exponential decrease of $f(\epsilon, t)$ but does not affect its spatial shape. Therefore, the spatial shape is given by the Bessel function $J_0(\lambda_1 \sqrt{\epsilon/\epsilon_{lim}})$ which has its maximum value at $\epsilon = 0$ and is monotonically decreasing with increasing ϵ for $\epsilon \leq \epsilon_{lim}$. Integrating Eq. (8) over ϵ , one finds the time dependent number of particles

$$N(t) \propto \exp \left[-\frac{\lambda_1^2}{4} \left(\frac{d\epsilon_{av}}{dt} \right) \frac{t}{\epsilon_{lim}} \right]. \quad (9)$$

Equations (8) and (9) show that for large t the time evolution of $f(\epsilon, t)$ and $N(t)$ do not depend on the initial particle distribution. However, in a real measurement a beam width smaller than the limiting aperture should be used, otherwise most of the particles will be lost before the memory of the initial beam shape can be washed out by the noise.

When Eq. (9) can be applied we find the expression

$$\epsilon_{lim} = \frac{\lambda_1^2}{4} \left(\frac{d\epsilon_{av}}{dt} \right) \tau_{loss}, \quad (10)$$

where

$$\tau_{loss} = (t_2 - t_1) \left[\ln \left(\frac{N(t_1)}{N(t_2)} \right) \right]^{-1} \quad (11)$$

is the characteristic loss time and t_1, t_2 are arbitrary moments.

B. Time dependent emittance

The time dependent averaged emittance ϵ_{av} written as a function of the revolution number n is

$$\epsilon_{av}(n) = \frac{1}{N_p} \sum_{p=1}^{N_p} \epsilon_p(n), \quad (12)$$

where

$$\epsilon_p(n) = \gamma_y y_{p,n}^2 + 2\alpha_y y_{p,n} y'_{p,n} + \beta_y y_{p,n}'^2 \quad (13)$$

is the emittance of the p th particle and $\alpha_y, \beta_y, \gamma_y$ are the Twiss parameters at the location of the source of the noise. The evolution of the phase space coordinates of a single particle follows

$$\begin{pmatrix} y_{p,1} \\ y'_{p,1} \end{pmatrix} = M \begin{pmatrix} y_{p,0} \\ y'_{p,0} + \Delta y'_{p,0} \end{pmatrix} = M \begin{pmatrix} y_{p,0} \\ y'_{p,0} \end{pmatrix} + M \begin{pmatrix} 0 \\ \Delta y'_{p,0} \end{pmatrix}, \quad (14)$$

where

$$M = \begin{pmatrix} \cos \mu + \alpha_y \sin \mu & \beta_y \sin \mu \\ -\frac{1+\alpha_y^2}{\beta_y} \sin \mu & \cos \mu - \alpha_y \sin \mu \end{pmatrix} \quad (15)$$

is the one turn map, and $\mu = 2\pi\nu_y$ is the phase advance of the betatron oscillation. $\Delta y'_{p,0}$ is the momentum kick due to

the noise. The characteristics of the noise are introduced later.

Iterating Eq. (14) yields the phase space coordinates of a single particle after n revolutions,

$$\begin{pmatrix} y_{p,n} \\ y'_{p,n} \end{pmatrix} = M^n \begin{pmatrix} y_{p,0} \\ y'_{p,0} \end{pmatrix} + \sum_{k=0}^{n-1} M^{n-k} \begin{pmatrix} 0 \\ \Delta y'_{p,k} \end{pmatrix}. \quad (16)$$

Using this equation, Eq. (12), and Eq. (13), we obtain

$$\begin{aligned} \epsilon_{av}(n) &= \frac{1}{N_p} \sum_{p=1}^{N_p} (y_{p,n}, y'_{p,n}) \cdot B \cdot \begin{pmatrix} y_{p,n} \\ y'_{p,n} \end{pmatrix} \\ &= \frac{1}{N_p} \sum_{p=1}^{N_p} \left\{ (y_{p,0}, y'_{p,0}) \cdot (M^n)^T \cdot B \cdot M^n \cdot \begin{pmatrix} y_{p,0} \\ y'_{p,0} \end{pmatrix} \right. \\ &\quad + \sum_{k=0}^{n-1} \left[(y_{p,0}, y'_{p,0}) \cdot (M^n)^T \cdot B \cdot M^{n-k} \cdot \begin{pmatrix} 0 \\ \Delta y'_{p,k} \end{pmatrix} \right. \\ &\quad \left. \left. + (0, \Delta y'_{p,k}) \cdot (M^{n-k})^T \cdot B \cdot M^n \begin{pmatrix} y_{p,0} \\ y'_{p,0} \end{pmatrix} \right] \right. \\ &\quad \left. + \sum_{k,l=0}^{n-1} (0, \Delta y'_{p,l}) \cdot (M^{n-l})^T \cdot B \cdot M^{n-k} \cdot \begin{pmatrix} 0 \\ \Delta y'_{p,k} \end{pmatrix} \right\}, \quad (17) \end{aligned}$$

where the upper index T denotes the transpose of a matrix. B is the beta matrix defined by

$$B = \begin{pmatrix} \frac{1+\alpha_y^2}{\beta_y} & \alpha_y \\ \alpha_y & \beta_y \end{pmatrix}. \quad (18)$$

The momentum kicks $\Delta y'_{p,k}$ in Eq. (17) are assumed to be uncorrelated with respect to the particle number p and the revolution number k . Hence, the kicks are entirely determined by a stationary single-kick distribution function $p_1(\Delta y')$. Under this assumption, the average of any function of the momentum kick, $g(\Delta y')$, can be approximated by

$$\int_{-\infty}^{\infty} g(\Delta y') p_1(\Delta y') d(\Delta y') = \frac{1}{N} \sum_{n=1}^N g(\Delta y'_n), \quad (19)$$

if N is sufficiently large. The mean value of the distribution function is assumed to be

$$\int_{-\infty}^{\infty} \Delta y' p_1(\Delta y') d(\Delta y') = 0, \quad (20)$$

and we define the mean square value

$$\int_{-\infty}^{\infty} (\Delta y')^2 p_1(\Delta y') d(\Delta y') = \sigma_{\Delta y'}^2. \quad (21)$$

Applying this in Eq. (17) leads to

$$\epsilon_{av}(n) = \epsilon_{av,0} + n \beta_y \sigma_{\Delta y'}^2. \quad (22)$$

The derivation of this formula is shown in Appendix A.

The time derivative of the averaged emittance given in Eq. (22) is

$$\frac{d\epsilon_{av}(t)}{dt} \Big|_{t=nT_0} \approx \frac{\epsilon_{av}(n+1) - \epsilon_{av}(n)}{T_0} = \frac{\beta_y \sigma_{\Delta y'}^2}{T_0}. \quad (23)$$

Here, T_0 is the revolution time. Using this result in Eq. (10), one finds

$$\epsilon_{lim} = \frac{\lambda_1^2}{4} \beta_y \sigma_{\Delta y'}^2 \frac{\tau_{loss}}{T_0}. \quad (24)$$

III. BEAM BEHAVIOR AFFECTED BY RF EXCITATION

A. The rf exciter

In the previous section we have discussed the growth of the beam width arising from particle diffusion driven by a purely stochastic force. In reality the force acting on the particles is, basically, a sinusoidal signal generated by an rf exciter. The basic parameters of the exciter as well as those of the beam and the lattice are presented in Table I. More details can be found in Ref. [10].

The exciter consists of two parallel plates with the distance d_0 between each other. Between them the voltage

$$U(t) = U_a \sin[2\pi f_c t + \phi_0(t)] \quad (25)$$

is generated, where f_c is the carrier or main frequency, and U_a is the amplitude voltage. The sinusoidal signal is modified by the phase $\phi_0(t)$. The phase is determined by a pseudorandom bit sequence, where it is $\phi_0 = \pi$ during a period when the bit status is 1 and $\phi_0 = 0$ otherwise. The duration of a bit status is $T_S = 1/f_S$, where f_S is the bit rate of the pseudorandom generator.

The power spectrum of the rf voltage is

$$P(f) \propto \frac{\sin^2[\pi(f - f_c)/f_S]}{[(f - f_c)/f_S]^2} + \frac{\sin^2[\pi(f + f_c)/f_S]}{[(f + f_c)/f_S]^2}. \quad (26)$$

TABLE I. Main experimental parameters.

Circumference of SIS-18 C	216.72 m
Working point ν_x, ν_y	4.17, 3.29
Ion	Ta ⁶¹⁺
Initial ion number $N_p(0)$	$\sim 10^9$
Particle energy E	(100, 200) MeV/u
Revolution time T_0 at (100, 200) MeV/u	(1.683, 1.273) μ s
Measuring time t_{max}	≈ 1.8 s
Resulting revolution number n	$\sim 10^6$
rms momentum width σ_p	5.0×10^{-4}
Nominal vertical chromaticity $\xi_{y,nat}$	-1.4647
Exciter length l_0	750 mm
Vertical exciter plate distance d_0	70 mm
Exciter amplitude voltage U_a	14.5 V and 29 V
Exciter frequency width f_S	$0.005/T_0$ and $0.01/T_0$
β_y at exciter position	7.0 m
α_y at exciter position	0.15

We omit the second term because it corresponds to negative frequencies. At $f = f_C \pm f_S$, one finds the zeros of $P(f)$ closest to the carrier frequency. So, f_S is the half width at zero spectral power density of the central peak of $P(f)$.

The voltage $U(t)$ leads to a time dependent, transverse electric field with an amplitude field strength

$$E_a = \frac{U_a}{d_0}. \quad (27)$$

Because the length of the exciter is much smaller than the length of a betatron period, the exciter acts approximately as a thin lens. Hence, the electric field creates in each revolution a momentum kick to the particles with a sinusoidal time behavior:

$$\Delta y'_n = \Delta y'_a \sin[n\psi_C + \phi_0(n)]. \quad (28)$$

Its amplitude value is

$$\Delta y'_a = \frac{qE_a \Delta t}{p}, \quad (29)$$

where q is the ion charge, p is the momentum, and Δt is the time needed by an ion to pass through the exciter. Using $q = Ze$, $\Delta t = l_0/(\beta_0 c)$, and $p = Am_u c \beta_0 \gamma_0$, this equation can be rewritten to

$$\Delta y'_a = \frac{e}{m_u c^2 \beta_0^2 \gamma_0} \frac{Z}{A} \frac{U_a l_0}{d_0}. \quad (30)$$

Here, $m_u c^2 = 931.5$ MeV is the rest energy of a nucleon, β_0, γ_0 are the relativistic factors, $l_0 = 750$ mm is the length of the exciter, $d_0 = 70$ mm is the distance between the plates, and Z, A are charge state and the mass number of the ions used.

In order to reach a maximum efficiency in beam excitation, the phase advance of the sinusoidal momentum kick is set to

$$\psi_C = 2\pi f_C T_0 = 2\pi \nu_{y,\text{frac}}, \quad (31)$$

because the excitation efficiency is approximately proportional to the spectral power density at $f = \nu_{y,\text{frac}}/T_0$.

The main difference with respect to the noise assumed in Sec. II is that the rf signal from the exciter generates the same momentum kick to all particles. Hence, the mean square value of the momentum kicks is

$$\sigma_{\Delta y'}^2 = \lim_{N \rightarrow \infty} \frac{1}{N} \sum_{n=0}^N (\Delta y'_n)^2. \quad (32)$$

The consequences of the application of such a momentum kick are discussed in the following section.

B. Emittance growth due to the rf signal

The major consequence of using an rf signal creating a uniform kick to all particles is that all particles will move coherently and independently of the particle density in phase space. Consequently, particle diffusion will not happen. Instead, the entire beam will randomly oscillate. On the other hand, the momentum spread $\delta = \Delta p/p$ will lead

TABLE II. Conditions used in the test tracking calculations presented in this section.

Particle energy E	100 MeV/u
Exciter amplitude voltage U_a	29 V
rms momentum uncertainty σ_p	0 and 5.0×10^{-4}
Chromaticity ξ_y	0, -0.01, -0.1, -1.0
Carrier frequency $f_C = \nu_{y,\text{frac}}/T_0$	172.3 kHz
Particles used in the simulations	1000, ..., 5000

to a spread in the particle tune, $\Delta \nu = \nu_y \xi_y \delta$, where ξ_y is the normalized chromaticity. Particle tracking simulations were performed to investigate the influence of this tune spread. The details of the tracking algorithm are introduced later; the parameters are presented in Table II. The simulations show that the oscillation of the beam center vanishes due to Landau damping when the tune spread is sufficiently large. The resulting beam profile has the maximum at the center and is monotonically decreasing with increasing radius, which was pointed out in Sec. II to be a consequence of particle motion driven by diffusion after a sufficiently long time. Additionally, chromaticity has a smoothing influence on the growth of the beam emittance $\epsilon_{av}(t)$, which one can see in Fig. 1. For $|\xi_y| > 0.1$, the emittance no longer depends on the chromaticity and is approximately a linear function of time, which is in qualitative agreement with Eq. (23). The quantitative differences resulting from the different types of noise are discussed in the next section.

IV. MODEL FOR PARTICLE TRACKING

The analytic model discussed in Sec. II is not applicable for the quantitative determination of the acceptance

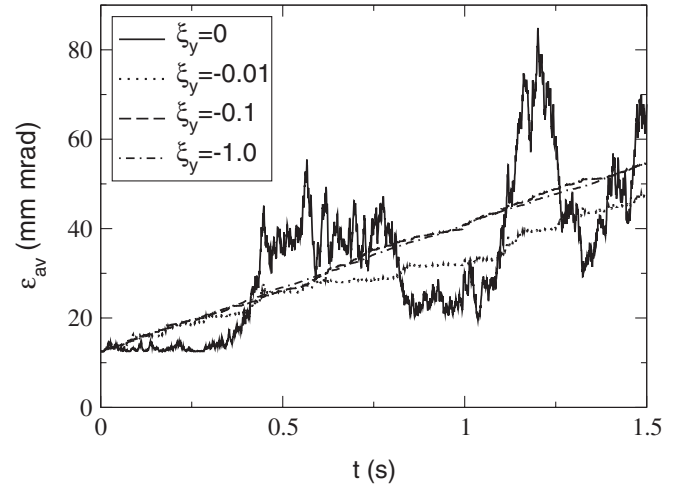


FIG. 1. Time evolution of the beam emittance calculated using the parameters from Table II depending on the chromaticity ξ_y . For $|\xi_y| > 0.1$ the growth of the emittance does not depend on chromaticity. Consequently, the curves for $\xi_y = -0.1$ and $\xi_y = -1$ are approximately identical.

because the real rf signal differs from white noise. Hence we study the problem numerically. The experiment is modeled by tracking particles through a lattice where a momentum kick identical to that of the rf exciter is applied to each particle for every turn. The time behavior of the beam emittance and the number of remaining particles are determined by assuming a test acceptance. The machine acceptance is obtained with a fitting procedure which varies the test acceptance until there is good agreement between the calculated and the measured particle number.

In our modeling we assume a linear lattice with decoupled horizontal and vertical particle motions. This enables us to use a one-dimensional model in our tracking calculations. We use a simplified lattice represented by the one turn map M defined in Eq. (15), so that the particle motion is given by Eq. (14). The momentum kick $\Delta y'_n$ has the sinusoidal time behavior given by Eq. (28). The initial particle coordinates are chosen according to a bi-Gaussian distribution in the vertical phase space and a Gaussian distribution in the longitudinal momentum space. That allows us to take into account the effect of the momentum spread in case of finite chromaticity. For this reason, the one turn map from Eq. (15) is modified to

$$M = M(\mu_p) = \begin{pmatrix} \cos\mu_p + \alpha_y \sin\mu_p & \beta_y \sin\mu_p \\ -\frac{1+\alpha_y^2}{\beta_y} \sin\mu_p & \cos\mu_p - \alpha_y \sin\mu_p \end{pmatrix} \quad (33)$$

with the modified phase advance,

$$\mu_p = \mu + \mu \xi_y \delta_p, \quad (34)$$

where δ_p is the individual momentum deviation of the p th particle. We assume $\delta_p = \text{const}$ because the beam is assumed to be coasting. α_y and β_y are assumed to be not affected by δ_p .

We benchmarked this model against the diffusion model presented in Sec. II. Here, we applied entirely stochastic momentum kicks to the particles to simulate diffusion due to white noise. In the comparison we found very good agreement between the tracking results and the analytic model. In particular, we found that the functional dependence between turn number $n = t/T_0$ and particle number $N(n)$ follows a scaling of $n\beta_y\sigma_{\Delta y}'^2/\epsilon_{\text{lim}}$ which agrees with Eq. (9), where Eq. (23) is inserted.

V. EXPERIMENTAL RESULTS AND THEIR EVALUATION

A. Model validation

As the first step, we perform a benchmarking test on the applicability of the diffusion model introduced in Sec. II. We apply a local bump to the closed orbit, thus shifting the beam by a defined displacement towards the aperture of the ring. This causes an artificial reduction of the acceptance and so faster particle loss. According to Eq. (10) we expect

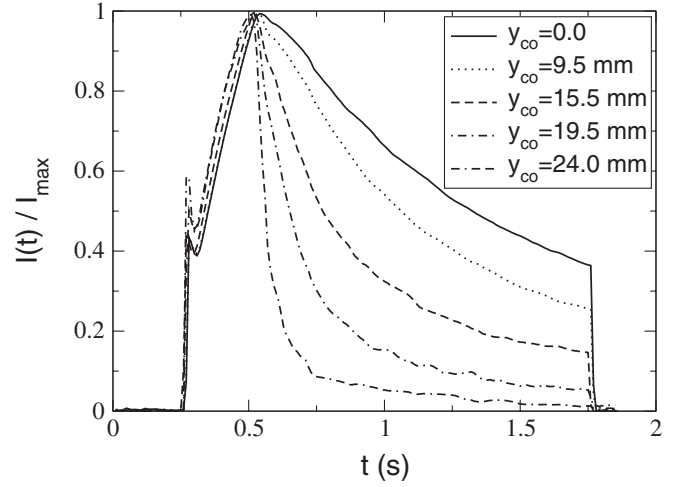


FIG. 2. Current as a function of time for different displacements due to the local closed orbit bump y_{co} . The injection starts at $t = 0.25$ s, the bump is applied from $t = 0.5$ s, and the beam is extracted at about $t = 1.8$ s. The exciter amplitude voltage $U_a = 29$ V, the half width of the power spectrum of the exciter [Eq. (26)] $f_S = 0.005/T_0$, and the beam energy $E = 100$ MeV/u were chosen.

a characteristic loss time $\tau_{\text{loss}} \propto \epsilon_{\text{lim}} \propto y_{\text{lim}}^2$, where y_{lim} is the limiting aperture. We present, here, results obtained for a beam energy $E = 100$ MeV/u and an exciter signal which has an amplitude voltage $U_a = 29$ V and a power spectrum with the half width $f_S = 0.005/T_0$ and the carrier frequency $f_C = \nu_{y,\text{frac}}/T_0$, where $\nu_{y,\text{frac}} = 0.29$. Figure 2 shows the current measured under these conditions as a function of time. The displacement of the closed orbit, y_{co} , measured at the location of a beam position monitor (BPM), $s = s_{\text{BPM}}$, and the resulting loss times τ_{loss} defined by Eq. (11) and normalized to the revolution time T_0 are presented in Table III.

The previous section showed that, in spite of the difference between the realistic rf signal and white noise, the averaged emittance grows linearly in time which yields an exponential decrease of the particle number, if the chromaticity is

TABLE III. Normalized loss times, τ_{loss}/T_0 , for $U_a = 29$ V, $f_S = 0.005/T_0$, and $E = 100$ MeV/u depending on the height of the closed orbit bump at the location of the beam position monitor, $s = s_{\text{BPM}}$. The loss times were determined from the duration of the time interval when $0.7I_{\text{max}} \geq I(t) \geq 0.4I_{\text{max}}$, see Fig. 2. The vertical beta function at s_{BPM} is assumed to be $\beta_y = 19.5$ m according to a calculation using MAD-X.

Index i	$y_{\text{co},i}/\text{mm}$	$\tau_{\text{loss},i}/T_0$
0	0	7.15×10^5
1	9.5	4.67×10^5
2	15.5	2.27×10^5
3	19.5	1.11×10^5
4	24.0	2.98×10^4

sufficiently large. This allows us to construct an analytical dependence between the displacement due to the closed orbit bump and the resulting loss times. We write Eq. (24) as

$$\epsilon_{\text{lim}} = \eta \frac{\tau_{\text{loss}}}{T_0}, \quad (35)$$

where η will be found with a regression analysis using the loss times, $\tau_{\text{loss},i}$, from Table III. If, furthermore, the closed orbit bump is large enough so that particle loss occurs basically only at its maximum position, $s = s_{\text{max}}$, we can replace the left-hand side of Eq. (35) by the acceptance reduced by the closed orbit bump given at s_{max} :

$$\epsilon_{\text{lim}}(y_{\text{co}}, s_{\text{max}}) = \frac{[y_{\text{lim}}(s_{\text{max}}) - y_{\text{co}}(s_{\text{max}})]^2}{\beta_y(s_{\text{max}})}, \quad (36)$$

where $y_{\text{lim}}(s_{\text{max}})$ is the limiting aperture at s_{max} . Expanding this expression and defining

$$\epsilon_{\text{lim},0}(s_{\text{max}}) = \frac{y_{\text{lim}}^2(s_{\text{max}})}{\beta_y(s_{\text{max}})} \quad (37)$$

yields

$$\begin{aligned} \epsilon_{\text{lim}}(y_{\text{co}}, s_{\text{max}}) &= \epsilon_{\text{lim},0}(s_{\text{max}}) - 2 \frac{y_{\text{lim}}(s_{\text{max}})}{\beta_y(s_{\text{max}})} y_{\text{co}}(s_{\text{max}}) \\ &\quad + \frac{y_{\text{co}}^2(s_{\text{max}})}{\beta_y(s_{\text{max}})}. \end{aligned} \quad (38)$$

Assuming the shape of the closed orbit bump is independent of its height it is

$$y_{\text{co}}(s_{\text{max}}) = A y_{\text{co}}(s_{\text{BPM}}), \quad (39)$$

where A is a constant. Using that in Eq. (38), and inserting Eq. (38) into Eq. (35), we find

$$c_0 + c_1 y_{\text{co}}(s_{\text{BPM}}) + c_2 y_{\text{co}}^2(s_{\text{BPM}}) = \frac{\tau_{\text{loss}}(y_{\text{co}})}{T_0} \quad (40)$$

with

$$\begin{aligned} c_0 &= \frac{\epsilon_{\text{lim},0}(s_{\text{max}})}{\eta}, \\ c_1 &= -2 \frac{A y_{\text{lim}}(s_{\text{max}})}{\eta \beta_y(s_{\text{max}})}, \quad \text{and} \quad c_2 = \frac{A^2}{\eta \beta_y(s_{\text{max}})}. \end{aligned} \quad (41)$$

The coefficients, c_0 , c_1 , c_2 , found with the quadratic regression are presented in Table IV. In the regression, the loss times for $y_{\text{co},0} = 0$ written in the first row of Table III are not used, because in this case it is unlikely that the particles have become lost at the position of the closed orbit bump. Figure 3 shows the resulting parabola compared to the loss times $\tau_{\text{loss},i}$. The parabola fits the loss times in good approximation. The relative regression error is

TABLE IV. Coefficients found from the quadratic regression.

c_0	1.023×10^6
$c_1(\text{m}^{-1})$	-6.9705×10^7
$c_2(\text{m}^{-2})$	1.1794×10^9

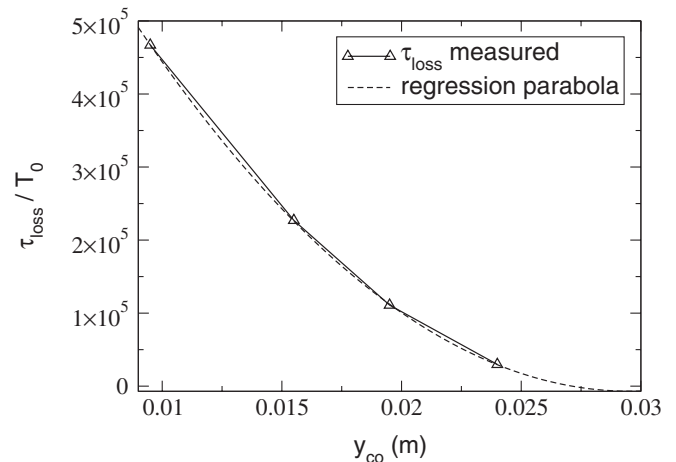


FIG. 3. Loss times determined from the measured current shown in Fig. 2 and the corresponding regression parabola as a function of the closed orbit bump $y_{\text{co},i}$ for $U_a = 29$ V, $f_S = 0.005/T_0$, and $E = 100$ MeV/u.

$$\begin{aligned} \Delta \tau_{\text{loss,rel}} &= \frac{\sqrt{\sum_{i=1}^4 (\tau_{\text{loss},i}/T_0 - c_0 - c_1 y_{\text{co},i} - c_2 y_{\text{co},i}^2)^2}}{\sqrt{\sum_{i=1}^4 (\tau_{\text{loss},i}/T_0)^2}} \\ &\approx 0.005. \end{aligned} \quad (42)$$

This result shows that the condition $\tau_{\text{loss}} \propto \epsilon_{\text{lim}}$ is fulfilled and thus the noise driven emittance growth in SIS-18 using our setup approximates very well the theory presented in Sec. II.

B. Determination of the acceptance

Finally, we apply the method introduced in Sec. IV to determine the acceptance of SIS-18. The experimental conditions are given by the parameters presented in Table I. The number of tracked particles is $N_p = 5000$. The number of revolutions is $n \approx 1.2 \times 10^6$ corresponding to a time interval of 2 s. We evaluate the experimental data measured for a beam energy $E = 100$ MeV/u, an exciter amplitude voltage $U_a = 29$ V, and two values of the width of the power spectrum of the exciter, $f_S = 0.005/T_0$ and $f_S = 0.01/T_0$.

To find the acceptance we set a test acceptance and simulate the time evolution of the beam current. With a trial-and-error procedure we repeat the simulation with the varied test acceptance until the curve for the particle number fits best the corresponding measured beam current. The test acceptance has been varied between 30 and 80 mm mrad.

To quantify the difference between measured and calculated particle number, the integral of the square of the difference between both curves for $t > t_0$ is determined. The instant t_0 must be large enough to be in the period of exponential particle loss introduced in Sec. II A. We found this requirement approximately fulfilled for $t_0 = 1.0$ s when $f_S = 0.01/T_0$ and for $t_0 = 0.75$ s when $f_S = 0.005/T_0$. The best agreement between measured and calculated

curves of the current is found for an acceptance $\epsilon_{\text{lim}} = 46$ mm mrad for $f_S = 0.01/T_0$ and $\epsilon_{\text{lim}} = 45$ mm mrad for $f_S = 0.005/T_0$. Performing an error analysis, we have estimated the maximum error due to uncertainties in the lattice and beam parameters to be smaller than 13%. The details of this analysis are presented in Appendix B.

VI. SUMMARY

We applied a vertical rf voltage to determine the vertical acceptance of the GSI heavy ion synchrotron, SIS-18. The excitation of the beam by the rf field led to an increase of the vertical beam size and to a reduction of the beam current when particles reached the aperture. We measured the beam current as a function of time and extracted the acceptance from the loss rate. The aim of this method was to remove the dependence of the measured data on the initial beam width.

The experimental data were quantitatively evaluated via particle tracking. First, we benchmarked the tracking method against an analytic model, where we used white noise in our numerical code and obtained very good agreement. To analyze the experimental data we applied the rf excitation used in the current measurements.

Finally, we determined the acceptance of SIS-18 using a trial-and-error procedure, where we repeated the simulations with many different test acceptances until we found one so that the resulting time evolution of the particle number fits the measured beam current.

In addition, we performed a numerical study where we varied beam and lattice parameters in order to estimate an upper limit for the acceptance error. We found that some of the parameter errors caused an acceptance error because the power spectrum of the exciter had a width f_S similar to the spread of the betatron frequency of the particles. For this reason, there is a betatron frequency dependence in the amount of excitation each particle receives because of the nonuniform power density. Consequently, we found that the modification of the acceptance due to the variation of these parameters depends on the width of the noise power spectrum. However, we did find nearly the same acceptance for different values of f_S . This suggests that the size of f_S does not dominate the acceptance error. We conclude that our method can reproduce the acceptance of an accelerator with an acceptable accuracy.

ACKNOWLEDGMENTS

We thank our colleagues O. Boine-Frankenheim and M. Kirk for helpful hints and discussions, and P. Kowina, W. Kaufmann, and C. Wetzel for help in the preparation and the usage of the exciter.

APPENDIX A: TIME EVOLUTION OF THE AVERAGED EMITTANCE DUE TO WHITE NOISE

In this Appendix, the time evolution of the beam emittance, ϵ_{av} , is calculated in terms of the number of

revolutions, $n = t/T_0$, where each particle experiences in every revolution a random momentum kick. As discussed in Sec. II B, these kicks are assumed to be uncorrelated with respect to the particle and the revolution. The starting point is Eq. (17),

$$\begin{aligned} \epsilon_{\text{av}}(n) = & \frac{1}{N_p} \sum_{p=1}^{N_p} \left\{ (y_{p,0}, y'_{p,0}) \cdot (M^n)^T \cdot B \cdot M^n \cdot \begin{pmatrix} y_{p,0} \\ y'_{p,0} \end{pmatrix} \right. \\ & + \sum_{k=0}^{n-1} \left[(y_{p,0}, y'_{p,0}) \cdot (M^n)^T \cdot B \cdot M^{n-k} \cdot \begin{pmatrix} 0 \\ \Delta y'_{p,k} \end{pmatrix} \right. \\ & \left. \left. + (0, \Delta y'_{p,k}) \cdot (M^{n-k})^T \cdot B \cdot M^n \begin{pmatrix} y_{p,0} \\ y'_{p,0} \end{pmatrix} \right] \right. \\ & \left. + \sum_{k,l=0}^{n-1} (0, \Delta y'_{p,l}) \cdot (M^{n-l})^T \cdot B \cdot M^{n-k} \cdot \begin{pmatrix} 0 \\ \Delta y'_{p,k} \end{pmatrix} \right\}, \end{aligned} \quad (\text{A1})$$

where

$$\begin{pmatrix} y_{p,n} \\ y'_{p,n} \end{pmatrix} = M^n \begin{pmatrix} y_0 \\ y'_0 \end{pmatrix} + \sum_{k=0}^{n-1} M^{n-k} \begin{pmatrix} 0 \\ \Delta y'_{p,k} \end{pmatrix} \quad (\text{A2})$$

is the phase space vector of the p th particle after n revolutions according to Eq. (16). The beta matrix B containing the Twiss functions reads

$$B = \begin{pmatrix} \frac{1+\alpha^2}{\beta} & \alpha \\ \alpha & \beta \end{pmatrix}. \quad (\text{A3})$$

In Eq. (A1), the matrix

$$M = \begin{pmatrix} \cos \mu + \alpha \sin \mu & \beta \sin \mu \\ -\frac{1+\alpha^2}{\beta} \sin \mu & \cos \mu - \alpha \sin \mu \end{pmatrix} \quad (\text{A4})$$

is a linear one turn map providing the time evolution of one particle during a single revolution.

The transformation of the phase space coordinates of a particle due to M does not change its emittance. Hence, the first term in the curly brackets in Eq. (A1) gives the initial beam emittance $\epsilon_{\text{av},0}$, and the change of the beam emittance during n revolutions,

$$\Delta \epsilon_{\text{av}}(n) = \epsilon_{\text{av}}(n) - \epsilon_{\text{av},0}, \quad (\text{A5})$$

arises from the sum over the second and the third term in the curly brackets in Eq. (A1).

The contribution arising from the terms in the square brackets in Eq. (A1) vanishes because, according to Eqs. (19) and (20),

$$\frac{1}{N_p} \sum_{p=1}^{N_p} \Delta y'_{p,k} = 0 \quad (\text{A6})$$

and the kicks $\Delta y'_{p,k}$ do not depend on the initial phase space coordinates of the particles $(y_{p,0}, y'_{p,0})$.

To perform the ensemble average of the last term in the curly brackets of Eq. (A1), the correlation function with respect to the revolution number,

$$\frac{1}{N_p} \sum_{p=1}^{N_p} \Delta y'_{p,l} \Delta y'_{p,k} = \sigma_{\Delta y'}^2 \delta_{lk}, \quad (\text{A7})$$

can be used, which approaches the mean squared value of the single-kick distribution $p_1(\Delta y')$ given in Eq. (21) when $l = k$ and $N_p \rightarrow \infty$. Therefore, we find that the change in beam emittance defined in Eq. (A5) is

$$\begin{aligned} \Delta \epsilon_{\text{av}}(n) &= \frac{1}{N_p} \sum_{p=1}^{N_p} \sum_{k=0}^{n-1} (0, \Delta y'_{p,k}) \cdot (M^{n-k})^T \cdot B \cdot M^{n-k} \cdot \begin{pmatrix} 0 \\ \Delta y'_{p,k} \end{pmatrix} \\ &= \sigma_{\Delta y'}^2 \sum_{k=0}^{n-1} (0, 1) \cdot (M^{n-k})^T \cdot B \cdot M^{n-k} \cdot \begin{pmatrix} 0 \\ 1 \end{pmatrix} \\ &= n \beta \sigma_{\Delta y'}^2. \end{aligned} \quad (\text{A8})$$

APPENDIX B: ERROR ESTIMATION

The lattice and beam parameters used in the calculations are standard values used in the machine control system, or they are based on a calculation done with MAD-X [11]. That implies there may be deviations of these parameters from those in the real machine.

In this analysis, we have to distinguish between random errors which can be different for different measurements under the same conditions and systematic errors which remain constant as long as the machine settings are not modified.

In the first step we investigate the random errors. Random errors lead to a spread of the measured curves of the current $I(t)$. Therefore, we estimate the random errors by direct comparison of all curves of $I(t)$ measured for the same parameters. These curves have been adjusted so that they pass through the same value at $t_0 = 1.0$ s for $f_S = 0.01/T_0$ and $t_0 = 0.75$ s for $f_S = 0.005/T_0$, where t_0 denotes approximately the beginning of the period of exponentially decreasing particle number. The maximum spread in $I(t)$ has always been found to be smaller than 1.0% which corresponds to an acceptance error up to $|\Delta \epsilon_{\text{lim,random}}| = 1$ mmrad or $\delta \epsilon_{\text{lim,random}} \equiv |\Delta \epsilon_{\text{lim,random}}| / \epsilon_{\text{lim}} = 0.02$.

To estimate the effect of systematic errors, we study numerically the dependence of the acceptance on the uncertainties of the parameters $X \equiv (\beta_y, \alpha_y, \sigma_p, \xi_y)$. In the study we add a maximum error ΔX to each parameter X_0 from Table I which we use to determine the acceptance, where only one of the parameters is changed for each simulation. Applying the trial-and-error procedure introduced in Sec. VB, we find the acceptance $\epsilon_{\text{lim}}(X_0 + \Delta X)$ so that the resulting particle number $N(t)$ fits the best $N(t)$ calculated from X_0 . The difference between $\epsilon_{\text{lim}}(X_0 + \Delta X)$

TABLE V. Variables and their assumed maximum systematic relative deviations.

Variable	Unperturbed value	Maximum relative error
	(see Table I)	$ \Delta X/X_0 _{\text{max}}$
β_y	7.0 m	10%
ξ_y	-1.4647	10%
σ_p	5×10^{-4}	10%

and $\epsilon_{\text{lim}}(X_0)$ is the systematic error arising from ΔX . The maximum relative errors $|\Delta X/X_0|_{\text{max}}$ are shown in Table V. We assume these errors to describe the worst case in order to find an upper limit for the acceptance error.

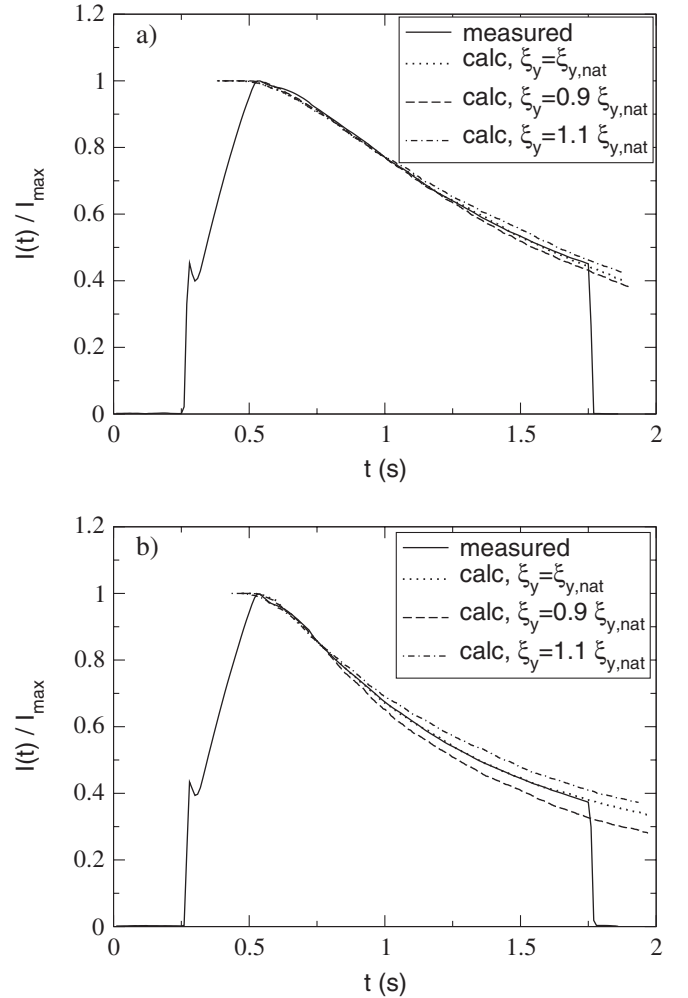


FIG. 4. Current as a function of time measured and computed for $U_a = 29$ V. In graph (a), the half width of the power spectrum of the exciter [Eq. (26)] is $f_S = 0.01/T_0$ and the acceptance is $\epsilon_{\text{lim}} = 46$ mmrad. In graph (b), $f_S = 0.005/T_0$ and $\epsilon_{\text{lim}} = 45$ mmrad are used. For both graphs the chromaticity has been varied by $\pm 10\%$ in the simulations. The resulting modifications of the beam current $I(t)$ at $t = 1.75$ s are $+4.5\%$ and -2.7% , respectively, in graph (a) and $+7.2\%$ and -14.5% , respectively, in graph (b).

The results obtained from the variation of α_y and β_y can be checked using a simplification of Eq. (17). Replacing the random momentum kick by that of the exciter given in Eq. (28) and the one turn map $M(\mu)$ by $M(\mu_p)$ according to Eq. (33), we find that the time evolution of the beam emittance is

$$\epsilon_{av}(n) = \epsilon_{av,0} + \frac{\beta_y}{N_p} \sum_{p=1}^{N_p} \sum_{k,l=1}^{n-1} \cos[(k-l)\mu_p] \Delta y'_k \Delta y'_l, \quad (\text{B1})$$

where $\mu_p = \mu + \mu \xi_y \delta_p$ is the phase advance of the p th particle per revolution. This equation shows that ϵ_{av} is independent of α_y and it is only a function of β_y . Therefore, there is no error for α_y in Table V. The predictions of Eq. (B1) are numerically confirmed to a high precision, i.e., the acceptance error due to the error in the beta function of 10% is

$$\delta \epsilon_{lim}(\Delta \beta_y) \equiv |\Delta \epsilon_{lim}(\Delta \beta_y) / \epsilon_{lim}| = 0.1. \quad (\text{B2})$$

The uncertainties of ξ_y and σ_p yield the uncertainty of the rms betatron tune of the particles $\Delta \nu_{rms} = \Delta(\nu_y \xi_y \sigma_p)$ that influences the growth of the beam emittance because the corresponding spread in the particle betatron frequencies is similar to the width of the noise power spectrum of the exciter f_S . That leads to a nonuniform spectral power density so that the excitation of a particle depends on its tune. Applying an error in ξ_y of $\pm 10\%$, we found that the resulting modification of the beam current $I(t)$ is strongly influenced by f_S , which one can see in Fig. 4. Consequently, the acceptance error is strongly influenced by f_S because the acceptance needs to be changed by -2.5 and $+3.7$ mm mrad, respectively, so that $N(t)$ fits the calculated curve when $f_S = 0.01/T_0$, whereas for $f_S = 0.005/T_0$ the change is ∓ 6.6 mm mrad. However, ϵ_{lim} must not depend on f_S and so the initial estimate for the error in ξ_y is too large. By reducing the chromaticity error to -4% , ϵ_{lim} becomes independent of f_S . Using this new error estimate for ξ_y , we find that $\epsilon_{lim} = 48$ mm mrad. The relative deviation of this value from the smaller acceptance calculated for unperturbed parameters, $\epsilon_{lim} = 45$ mm mrad, is

$$\delta \epsilon_{lim}[\Delta(\xi_y \sigma_p)] \equiv |\Delta \epsilon_{lim}[\Delta(\xi_y \sigma_p)] / \epsilon_{lim}| = 0.067. \quad (\text{B3})$$

If the uncertainties in β_y and $\xi_y \sigma_p$ are independent then the resulting total acceptance error is $|\Delta \epsilon_{lim} / \epsilon_{lim}|_{tot} = \sqrt{[\delta \epsilon_{lim,random}]^2 + [\delta \epsilon_{lim}(\Delta \beta_y)]^2 + \{\delta \epsilon_{lim}[\Delta(\xi_y \sigma_p)]\}^2} < 0.13$. According to the values for the acceptance in the previous section, ϵ_{lim} is between 40 and 52 mm mrad.

-
- [1] Parameter list of SIS-18: http://www.gsi.de/beschleuniger/sis18/pdf/sis18_parameterliste.pdf.
 - [2] P. Spiller and G. Franchetti, *Nucl. Instrum. Methods Phys. Res., Sect. A* **561**, 305 (2006).
 - [3] "An International Accelerator Facility for Beams of Ions and Antiprotons," Conceptual design report, GSI Darmstadt, 2006, Section 3, "The Facility," <http://www.gsi.de/GSI-Future/cdr>.
 - [4] E. Mustafin, O. Boine-Frankenheim, I. Hofmann, H. Reich-Sprenger, and P. Spiller, *Nucl. Instrum. Methods Phys. Res., Sect. A* **510**, 199 (2003).
 - [5] C. Omet, P. Spiller, J. Stadlmann, and D. H. H. Hoffmann, *New J. Phys.* **8**, 284 (2006).
 - [6] A. Parfenova and G. Franchetti, in *Proceedings of the 23rd Particle Accelerator Conference, Vancouver, Canada, 2009* (IEEE, Piscataway, NJ, 2009), TH6PFP053, p. 3826.
 - [7] X. L. Zhang, V. Shiltsev, and C. Y. Tan, in *Proceedings of the 21st Particle Accelerator Conference, Knoxville, 2005* (IEEE, Piscataway, NJ, 2005), p. 2306.
 - [8] X. Altuna, A. Arimatea, R. Bailey, T. Bohl, D. Brandt, K. Cornelis, C. Depas, F. Gallucio, J. Gareyte, R. Giachino, M. Giovannozzi, Z. Guo, W. Herr, A. Hilaire, T. Lundberg, J. Miles, L. Normann, T. Risselada, W. Scandale, F. Schmidt, A. Spinks, and M. Venturini, *The 1991 Dynamic Aperture Experiment at the CERN SPS*, in AIP Conf. Proc. No. 255 (AIP, New York, 1991), p. 355.
 - [9] D. A. Edwards and M. Syphers, *An Introduction to the Physics of High Energy Accelerators* (Wiley, New York, 1993).
 - [10] M. Kirk and P. Moritz, GSI Internal Note, GSI Darmstadt, 2006.
 - [11] MAD-X code, see <http://mad.web.cern.ch/mad>.